SCIENTIFIC REPORTS

OPEN

SUBJECT AREAS:
BATTERIES
TWO-DIMENSIONAL MATERIALS
ELECTRONIC DEVICES

Received
25 June 2014

Accepted
21 November 2014

Published
10 December 2014

Correspondence and requests for materials should be addressed to Z.T. (zirong@hust.edu.cn)

Growth of Hierarchal Mesoporous NiO Nanosheets on Carbon Cloth as Binder-free Anodes for High-performance Flexible Lithium-ion Batteries

Hu Long[1], Tielin Shi[1,2], Hao Hu[1], Shulan Jiang[1], Shuang Xi[1] & Zirong Tang[1,2]

[1]State Key Laboratory of Digital Manufacturing Equipment and Technology, Huazhong University of Science and Technology, Wuhan 430074, China, [2]Wuhan National Laboratory for Optoelectronics, Huazhong University of Science and Technology, Wuhan 430074, China.

Mesoporous NiO nanosheets were directly grown on three-dimensional (3D) carbon cloth substrate, which can be used as binder-free anode for lithium-ion batteries (LIBs). These mesoporous nanosheets were interconnected with each other and forming a network with interval voids, which give rise to large surface area and efficient buffering of the volume change. The integrated hierarchical electrode maintains all the advantageous features of directly building two-dimensional (2D) nanostructues on 3D conductive substrate, such as short diffusion length, strain relaxation and fast electron transport. As the LIB anode, it presents a high reversible capacity of 892.6 mAh g^{-1} after 120 cycles at a current density of 100 mA g^{-1} and 758.1 mAh g^{-1} at a high charging rate of 700 mA g^{-1} after 150 cycles. As demonstrated in this work, the hierarchical NiO nanosheets/carbon cloth also shows high flexibility, which can be directly used as the anode to build flexible LIBs. The introduced facile and low-cost method to prepare NiO nanosheets on flexible and conductive carbon cloth substrate is promising for the fabrication of high performance energy storage devices, especially for next-generation wearable electronic devices.

Energy conversion and storage is undoubtedly one of the greatest challenges in today's world[1]. Lithium ion batteries (LIBs), a fast-developing technology in electric energy storage, are currently predominant for a wide range of portable electronic devices, because of their advantages of high energy density, long cycle life, and environmental benignity[1,2]. In response to the emerging need, it is still essential to develop alternatives for commercially available LIBs electrode materials due to their low capacity and poor rate capability[1–3]. Nowadays, research efforts have been focused on discovering potential materials and fabrication techniques for developing the next-generation LIBs electrodes[3–6]. Nanostructured materials have attracted great interest in recent years because of the short diffusion lengths of li-ions, large material/electrolyte contact area, good strain accommodation, and the unusual mechanical and electrical properties endowed by confining the dimensions[4–9].

Recently, nano-sized transition metal oxides have been widely studied as anode materials for LIB applications owing to their high theoretical specific capacities and volumetric energy densities, comparing to the commercial graphite anode (372 mAh g^{-1})[3,9–16]. Among them, nickel oxide (NiO) has attracted considerable attention due to its natural abundance, low cost, environmental friendliness, and high theoretical capacity (718 mAh g^{-1})[10,16–30]. Moreover, NiO may result in a high volumetric energy density due to its high density of 6.67 g cm^{-2}. All of these impressive properties make it promising candidate as anode material in LIBs. Nevertheless, like other conversion based anode materials, the potential of utilizing NiO as high power LIB anode is greatly hindered by its poor electronic conductivity and capacity retention performance. To circumvent these problems, several research developments have been demonstrated recently, such as synthesis of NiO with nanostructures including nanotubes[16], nanofibers[17,18], nanoparticles[19], nanosheet-based microspheres[20,21], nanoflakes[22], nanoplates[23] and nanospheres[24] as well as forming composites with conductive materials like carbon and graphene[25–30]. In particular, the porous nanosheets based structure is considered as promising due to its porous structures and large specific

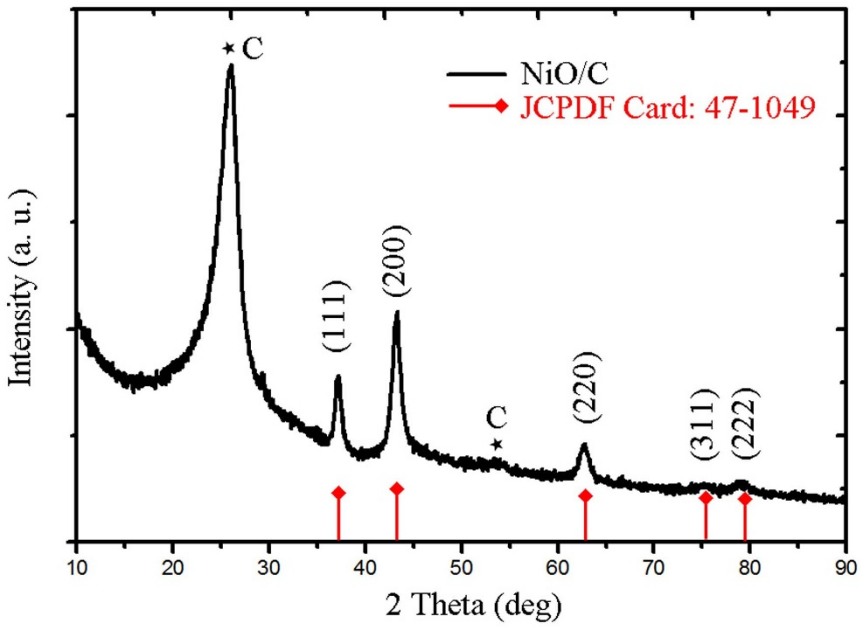

Figure 1 | XRD pattern of the as-prepared NiO/carbon cloth composite.

surface areas, which can provide a short and easier pathway for electrolyte and ions to enhance their electrochemical performance. Notwithstanding these advances, the rational design and controllable synthesis to high performance anode still remain as significant challenges[20,21].

Currently, 3D electroactive nanostructured materials grown directly on conductive substrates as binder-free integrated electrodes for LIBs is an emerging new concept to bypass the problems, which can not only avoid the "dead surface" in traditional slurry-derived electrodes and allow for more efficient electron transport but also simplify electrode processing[31–33]. Moreover, the free space within nanostructures can better accommodate the volume change of the entire electrode during lithium insertion/extraction[31]. There have been several reports of direct growth of nanostructured electroactive metal oxides on conductive substrates to improve LIBs performance[31–35]. For example, $ZnCo_2O_4$ nanowire self-assembled hierarchical structures were synthesized on 3D conductive Ni foam substrate in our previous work, which presented enhanced lithium storage performance[34]. The direct growth of aligned single-crystalline NiO nanoflake arrays on Cu foils also shows a capacity of 720 mAh g^{-1} after 20 cycles[35]. Besides the above, the commercially available carbon cloth is considered as a new kind of substrate, which possesses the advantages of 3D structures, high conductivity, high strength, good corrosion resistance and high flexibility. Very recently, one-dimensional (1D) $ZnCo_2O_4$ nanowires grown on carbon cloth have been reported as flexible anode for LIBs, showing that growing nanostructured materials on carbon cloth is a promising strategy for flexible battery configuration[36–38].

Inspired by these advances, herein we report a cost-effective method to direct grow NiO nanostructures on flexible carbon cloth. The obtained nanostructures are mesoporous and have unique ultrathin sheet-like feature. These mesoporous nanosheets are interconnected with each other forming a stable network over the carbon cloth. Using the mesoporous NiO nanosheets/carbon cloth as a binder-free LIB anode, the integrated electrode exhibited high capacity, excellent cycling performance and good rate capability, which provides a possibility to replace graphite material. We further assembled a flexible full LIB to light a commercial LED light and four lighting nixie tubes under bending state, which demonstrates their potential applications in flexible electronics. And, to the best of our knowledge, the NiO nanostructure-based flexible electrodes have not yet been reported.

Result

In this study, ultrathin NiO nanosheets were successfully prepared on carbon cloth via a hydrothermal synthesis and subsequent annealing treatment. The composition and phase purity of the as-prepared samples were examined by X-ray diffraction (XRD), which are shown in Figure 1, Figure S1 and Figure S2. As shown in Figure S1, the diffraction peaks of the as-prepared precursor/carbon cloth can be assigned to $Ni(OH)_2 \cdot 0.75H_2O$ (JCPDS 38-0715) and $Ni(OH)_2$ (JCPDS 14-0117). After being annealed at 350°C for 2 h, the NiO-precursor is completely transformed to the cubic NiO phase (JCPDS 47-1049). As shown in Figure 1, all the diffraction peaks in the pattern can be indexed to NiO with the face-centered cubic phase (JCPDS 47-1049). Besides, the observed peaks at 26° and 54° can be ascribed to the carbon cloth substrate, which can also be observed in the XRD pattern of pure carbon cloth as shown in Supplementary Figure S2. No additional diffraction peaks other than NiO and carbon were detectable, implying the high purity of the product.

The SEM image of the pure carbon cloth is shown in Supplementary Figure 3S(a), which exhibits the ordered texture structure. Magnified image in Supplementary Figure 3S(b) illustrates that each carbon fiber with smooth surface has a uniform diameter of around 10 μm. Figure 2 shows the morphology of the as-prepared NiO nanosheets/carbon cloth. Figure 2a is the low-magnification SEM image of the final product, showing that the ordered woven structure of the carbon cloth still remains. The inset figure shows the optical images of the carbon cloth before and after NiO growth. It can be observed that the pure carbon cloth is with deep black color while the NiO nanosheets/carbon cloth is with light green color. Figure 2b clearly displays the well-established texture structure of the NiO nanosheets grown on the carbon fibers. From the enlarged view shown in Figure 2c, it can be observed that the nanosheets are grown perpendicularly over the entire carbon fiber. The nanosheets are interconnected with each other, which can not only create porous nanostructure with abundant open space and electroactive surface, but also buffer the volume change resulted from both external bending stress and repeated Li^+ insertion–extraction. The free space between nanosheets will be beneficial for the diffusion of electrolyte

into the electrode, leading to reduced diffusion lengths of Li-ions. The thickness of the NiO nanosheets layer is about 1.3 μm, which can be clearly observed in the Figure 4S. In average, the mass loading of NiO nanosheets is about 1.77 mg on 1 cm^2. Thus, a higher energy density can be achieved by the direct growth of nanostructures on conductive substrate compared to traditional binder based-electrode.

The mesoporous feature of the NiO nanosheets is clearly revealed through transmission electron microscopy (TEM) analysis, as shown in Figure 3. Figure 3a shows the low-magnification TEM image of one-piece prepared NiO nanosheets peeled off from the carbon fiber. The NiO nanosheets exhibit folding silk-like morphology with transparent feature, indicating their ultrathin nature. Due to the much larger lateral size than the thickness, the morphologies of bending, curling, and crumpling are clearly observed. The dark strips are generally the folded edges or wrinkles of the nanosheets, suggesting the interconnected nature of the sample, which is consistent with the SEM observations. The enlarged image shown in Figure 3b reveals that the nanosheets are around 2–10 nm in thickness. The ultrathin feature of the nanosheets is ideal for intercalation-based electrode materials because of the high surface area and small crystallites inside the ultrathin nanosheets as well as the short Li-ion diffusion path. The high-resolution TEM image of nanosheets is shown in Figure 3c. The lattice spacing of 0.24 nm and 0.21 nm can be readily indexed to the (111) and (200) crystal planes of the cubic NiO phase respectively, which further confirms the formation of crystalline structure of NiO nanosheets. The corresponding selected-area electron diffraction (SAED) pattern shown in Figure 3d indicates the polycrystalline nature of NiO. The diffraction rings are respectively assigned to (111), (200), (220), (311), (222), and (400) planes, which are in good agreement with the above XRD results. Moreover, numerous interparticle mesopores, distributed throughout the whole surface of these ultrathin nanosheets, can be clearly seen from Figure 3b. The inset image in Figure 3b indicates that the mesopore in nanosheets is with a pore size of around 2–5 nm, which could be related to the rapid release of water molecules during the annealing process. The mesoporous structures in nanosheets are important to facilitate the mass transport of electrolytes within the electrodes during fast discharging/charging process, to reduce the diffusion lengths of Li-ions and enable the achievement of durable high rate capability.

The mesoporous feature of NiO nanosheets was further characterized by BET N_2 adsorption–desorption analysis at 77 K. The nitrogen adsorption/desorption isotherms and pore size distribution in the nanostructures are shown in Figure 4. The as-prepared sample exhibits a specific surface area of 67.3225 $m^2\ g^{-1}$. The pore size distribution, derived from desorption data and calculated from the isotherm using the Barrett-Joyner-Halenda (BJH) model (the inset of Figure 4), shows that most of the pores fall into the size range of 2 to 5 nm and the average pore size is calculated to be 4.8 nm, which is in good agreement with the measured results of the high resolution TEM image. We further conducted the low-angle XRD test for NiO nanosheets/carbon cloth, and the result is shown in Figure S5. The absence of prominent peaks in the low-angle range indicates that the NiO nanosheets are with disordered mesoporosity. As demonstrated in many cases, the incorporation of mesoporosity in transition metal oxides, which can confine d-electrons to the walls

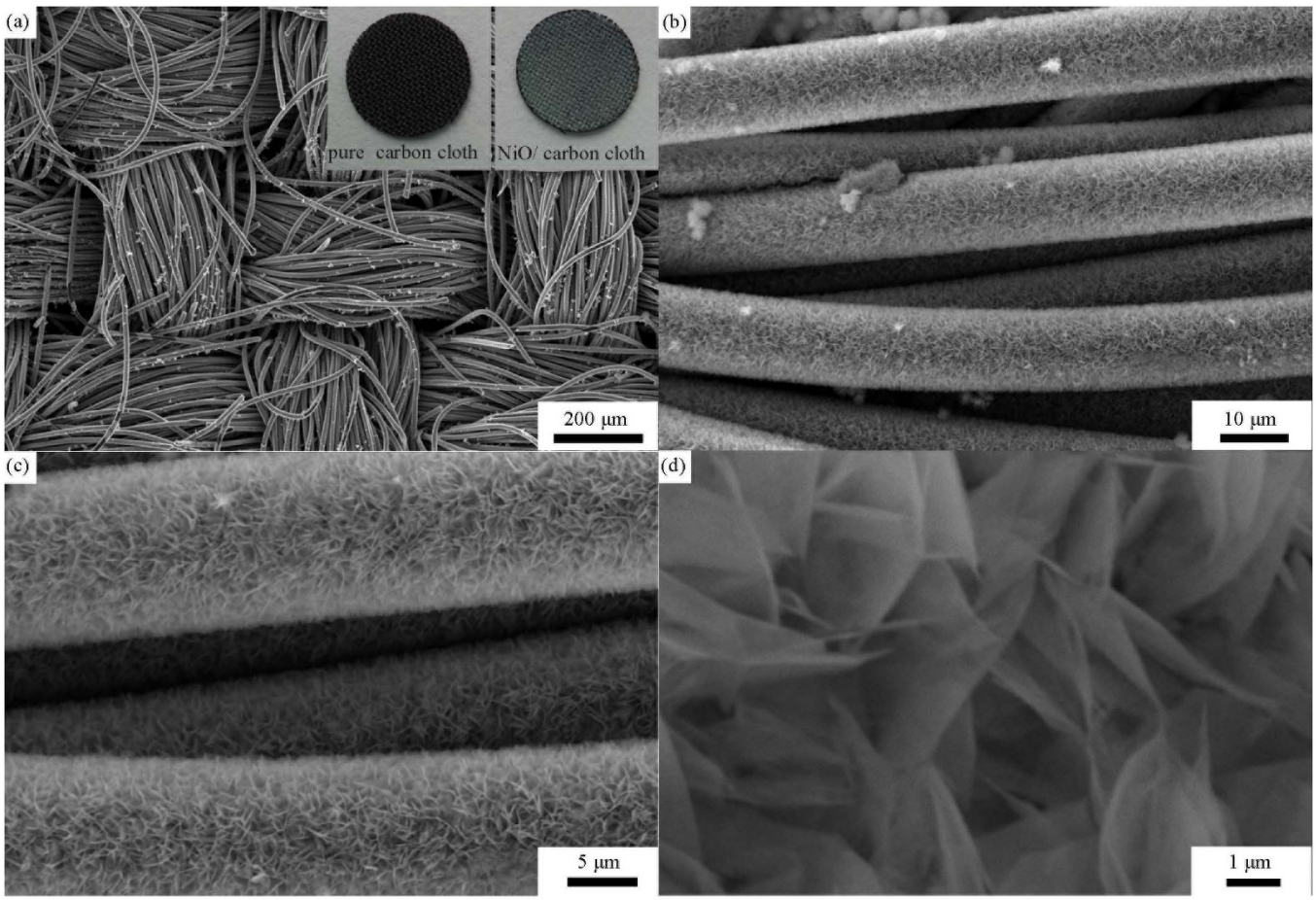

Figure 2 | Morphology of the as-prepared NiO/carbon cloth composite. (a–d) Typical SEM images of NiO nanosheets grown on carbon cloth with well-established textiles at different magnifications; Inset in Figure 2(a): the photographic images of carbon cloth before and after NiO nanosheets' growth.

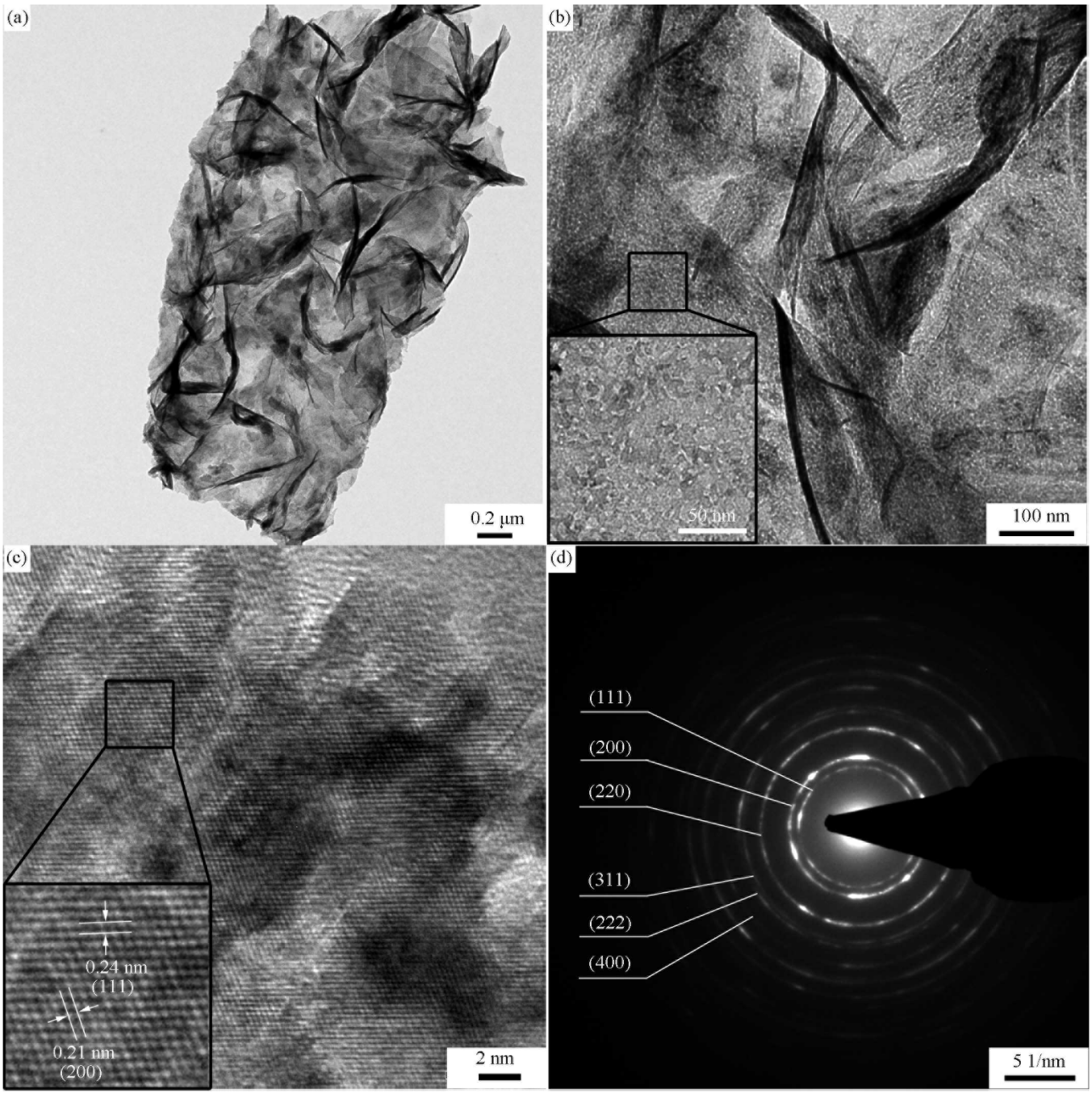

Figure 3 | TEM images and corresponding SAED pattern of NiO nanosheets. (a) Low-magnification TEM pattern of the as-prepared NiO structure peeled off from the carbon cloth. (b) Magnified TEM image of the NiO nanosheets. Inset: magnified image of the selected part showing the mesoporous feature of the NiO nanosheets. (c) High resolution TEM image of the nanosheets indicating the lattice spacing of 0.24 nm and 0.21 nm. (d) The corresponding SEAD pattern.

between the pores, brings improved electrochemical properties[39]. Such a mesoporous textural feature of NiO nanosheets will provide good access for Li-ions across the interface, rapid ion transport, and alleviate the mechanical strain owing to the volume variations during the repeated Li^+ insertion–extraction, which will be beneficial to the improvement of electrochemical performance.

To highlight the merits of the unique architecture, the mesoporous NiO nanosheets/carbon cloth was evaluated directly as an anode for LIBs. The as-prepared samples were configured in laboratory-based CR2032 coin-type half-cells, without any binders or conducting additives. To understand the reaction mechanism during electrochemical charge–discharge process, cyclic voltammograms (CV) tests were conducted at a voltage window of 0.01–3.0 V vs. Li^+/Li at a slow scan rate of 0.1 mV s^{-1}, as displayed in Figure S6. During the first cathodic sweep, two peaks are observed at around 0.67 V and 1.85 V. The strong peak at 0.67 V can be assigned to the reduction of NiO to Ni accompanied by the formation of amorphous Li_2O and electrolyte decomposition to form the solid electrolyte interphase (SEI) layer[20–24]. The relatively weak peak at 1.85 V might be attributed to the structural destruction and disappears in the subsequent scans. Different from the first cycle, the second cycle shows that the reduction peak is gradually moved to about 0.9 V and becomes much broader. In the anodic polarization process, a broad peak was observed between 1.15 V and 1.70 V, which can be attributed to

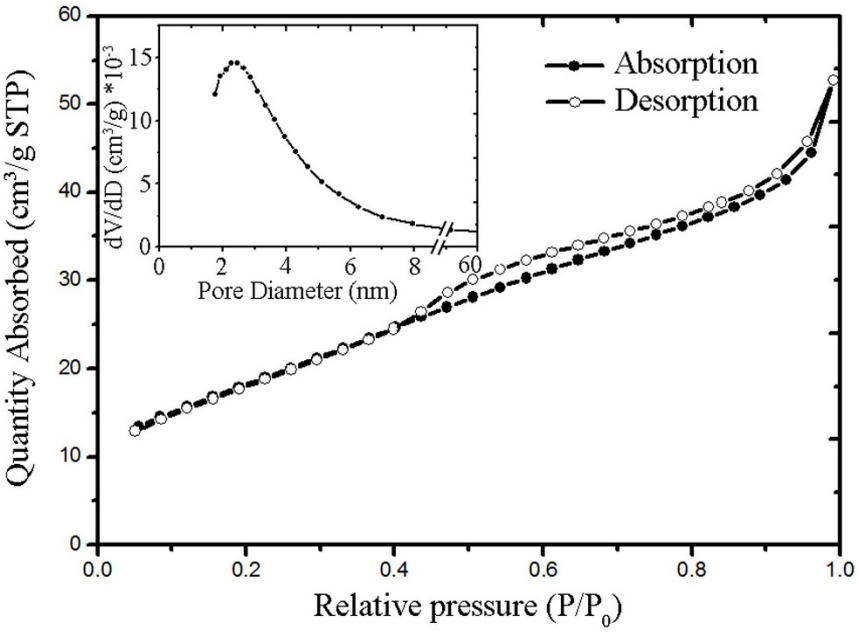

Figure 4 | Nitrogen adsorption and desorption isotherms of the NiO structure. Inset: corresponding pore distribution derived from Absorption data and calculated from the isotherm using the BJH model.

the dissolution of the SEI layer. The peak at 2.47 V is attributed to the oxidation of Ni to Ni^{2+}. The Nyquist plot of the mesoporous NiO nanosheets/carbon cloth electrode before cycles was exhibited in Figure S7. Based on the equivalent electrical circuit model shown in inset figure of Figure S7, the solution resistances (Rs) and the calculated charge transfer resistances (Rct) of the cells are 8.41 Ω and 54.5 Ω, respectively. The surface layer resistance is obviously small, which can benefit the diffusion of the Li ions.

Galvanostatic discharging-charging tests were performed to investigate the lithium insertion/extraction behavior of the prepared electrodes at a voltage window of 0.01–3 V vs Li^+/Li, and the electrochemical performance is presented in Figure 5. Figure 5(a) shows the representative discharging-charging profiles including 1st, 2nd, 10th and 60th cycle during discharging (Li^+ insertion) and charging (Li^+ extraction) process at a current rate of 100 mA g^{-1} (0.17C, C = 718 mA g^{-1}). It can be seen that the curve of first discharging process exhibits a wide plateau at about 0.7 V. In the following cycles, the discharging plateau becomes steeper and moves upward, and is replaced by a long sloping curve from 1.5 V to 0.9 V, which is similar to the previous reports[17–24]. The first charging curve exhibits two peaks at 1.6 V and 2.3 V, which can be assigned to the oxidation of SEI layer and Ni nanograins respectively[40–42]. This result is in good agreement with the CV measurements.

Figure 5(b) shows the capacity retention of the mesoporous NiO electrode at 100 mA g^{-1} and the corresponding Coulombic efficiencies. As expected, the attractive electrode architecture manifests good electrochemical reversibility and stability in the lithium insertion and extraction reactions. The initial discharging-charging capacities are 1156.5 and 882.6 mAh g^{-1} respectively, corresponding to a Coulombic efficiency of 76.3%. The irreversible capacity loss of 23.7% could be ascribed to electrolyte decomposition and irreversible formation of SEI films, which is lower than the most results of reported NiO electrodes[17–24]. The carbon substrate with good conductivity and the mesoporous sheet-like nanostructures should be responsible for the improvement in initial irreversible capacity loss. The discharging-charging capacities are kept well during the subsequent cycling without remarkable decay. A reversible capacity of 892.6 mAh g^{-1} was achieved even after 120 cycles with 103.4% capacity retention from 3 to 120 cycles. The discharging capacity is always higher than the theoretical capacity (718 mAh g^{-1}). This extra capacity may be ascribed to the reversible growth of a polymeric gel-like films resulted from kinetically activated electrolyte degradation, which is common in almost all transition metal oxide anodes[31,32,34,37–44]. Besides, the Columbic efficiencies are higher than 98% during 2 to 120 cycles indicating very good reversible capacity and cycling stability during the discharging and charging process. As shown in Figure S8, We further checked the structure of mesoporous NiO nanosheets/carbon cloth cycled at 100 mAh g^{-1} after 80 cycles. From the image, we can see that although some cracks were observed, the electrode still remains integrity, further proving the stability of the electrodes after cycling tests. To investigate the contribution of carbon cloth to the total capacity, galvanostatic discharging-charging tests were conducted, and the results are presented in Figure S9. It can be seen that the carbon cloth exhibits a negligible contribution to the total capacity of the mesoporous NiO nanosheets/carbon anode.

To evaluate the rate capability, the electrode was cycled at different current densities ranging from 100 to 5000 mA g^{-1} and the results are displayed in Figure 5c. As the current density was gradually increased from 100 to 250, 500, 1000, 2000 and 5000 mA g^{-1}, the electrode delivered the reversible capacity of 896.6, 782.5, 725.2, 584.8, 426 and 298.4 mAh g^{-1} respectively, which demonstrates an excellent high rate performance for high power LIBs. More importantly, after the high rate discharging-charging cycles, the discharging capacity could be resumed to 836.2 mAh g^{-1} and got an increase for another 10 cycles when the current density was performed at 100 mA g^{-1}. This indicates that the integrity of mesoporous NiO crystals has been preserved even after high rate cycling, showing a potential for high power application. Inspired by this, we further tested the mesoporous NiO electrode at a relative high current density of 700 mA g^{-1} (0.97C) for 150 cycles, as shown in Figure 5d. The electrode shows a slight decrease at the initial 30 cycles. Afterwards, the capacity gradually increases until the 150th cycle. The specific capacity remains at 758.1 mAh g^{-1} even after 150 cycles, which is higher than the theoretical capacity of 718 mAh g^{-1}. Besides, the Columbic efficiency of the first cycle is 85.3%, which is the highest in reported results of NiO electrodes. The good conductivity of the NiO/carbon cloth and unique structure of NiO with mesoporous sheet-like feature should be responsible for the improvement in initial irreversible capacity loss. The mesoporous nanosheet can promote accessibility of the electrolyte and diffusion of the species.

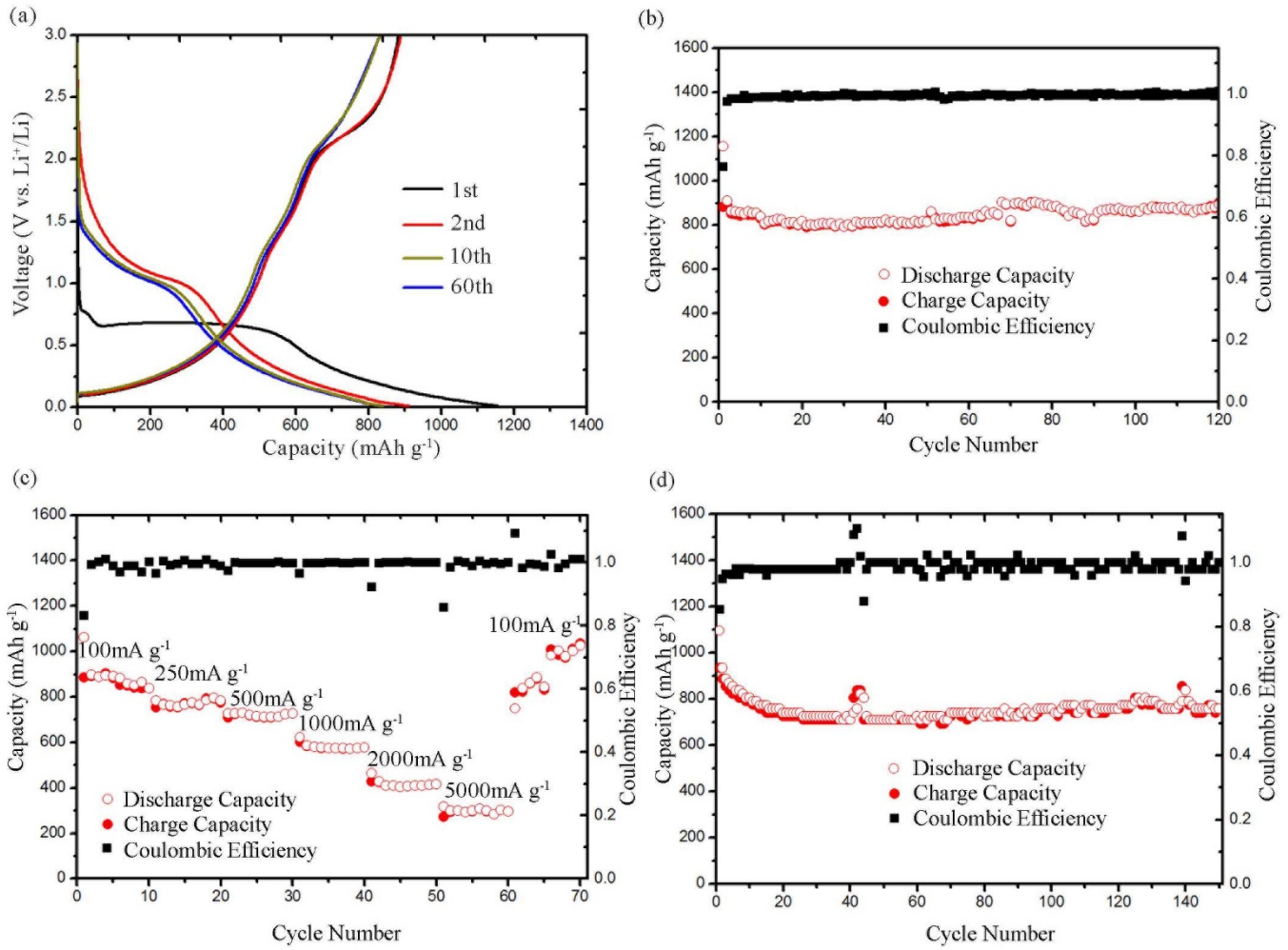

Figure 5 | Electrochemical characterizations of NiO nanosheets/carbon cloth based half-cells. (a) Representative galvanostatic discharging-charging voltage profiles at a current density of 100 mA g^{-1} in the voltage range of 0.01–3 V; (b) Capacity versus cycle numbers at 100 mA g^{-1} and the corresponding Coulombic efficiencies; (c) The rate performance of the electrode at various current densities. (d) Capacity of the electrode versus cycle numbers at the current density of 700 mA g^{-1} and the corresponding Coulombic efficiencies.

Moreover, the mesoporous NiO could promote the formation of highly disordered Ni nanograins which can implement the catalytic activity of the reduction and oxidation of the electrolyte, thus improving the initial Columbic efficiency and increasing the capacity[23]. Until now, this is the best high-rate cycling results under high current density with such a large mass loading without binder.

Discussion

The high capacity, excellent cycling stability and great rate capability of binder-free electrode based on the mesoporous NiO nanosheets/carbon cloth might be attributed to the following aspects. Firstly, the mesoporous feature of the NiO nanosheets demonstrated by TEM and BET results can not only provide a short distance for Li-ion diffusion and sufficient space for a high rate lithium intercalation, but also can effectively accommodate the large volume changes during the lithiation and delithiation process, thus leading to improved lithium storage properties[45]. Secondly, the interconnected nanosheets form a network texture and provide large active electrode–electrolyte contact area for high-speed access of Li-ions across the interface and good structural buffering against volume change. And the ultrathin nature of the nanosheets requires lower activation energy for the Li-ion intercalation reaction, which promotes the diffusion of electrolyte into the inner area of the electrode and enables rapid Li-ion diffusion. Thirdly, the highly conductive carbon cloth can greatly enhances the stability of the anode[36–38]. The direct growth of mesoporous NiO nanosheets on conductive carbon cloth substrate and their excellent adhesion provide a better electrical contact between NiO nanosheets and the substrate as well as fast electron transport, which is beneficial to improve the kinetics of the anode. Combining the integrated electrode design of interconnected NiO nanosheets grown on conductive substrates, the sheet-like ultrathin nanostructures, mesoporous feature of the NiO nanosheets will undoubtedly lead to enhanced electrochemical performance for high performance LIBs, which also offers a promising route for electrode design with high capacity, excellent cycling stability and rate capability for LIBs.

The mesoporous NiO nanosheets/carbon cloth electrodes showing excellent electrochemical performance also possess highly flexible characteristics, which make them suitable candidates for flexible electronic applications. Figure 6(a) shows the photographic images of bent carbon fiber cloth, revealing its highly flexible nature. Figure 6(b) shows the carbon cloth grown with mesoporous NiO nanosheets, which is also readily rolled up with a tweezer. It can be clearly observed that the integrated structure exhibits excellent flexibility, which makes it possible for further flexible device applications. To demonstrate its practical applications, we fabricated flexible full LIBs using the mesoporous NiO nanosheets/carbon cloth as binder-free anodes. Figure 6(c) shows the schematic of the fabricated flexible full battery, consisted of the flexible NiO nanosheets/carbon cloth (anode), a flexible separator, the $LiCoO_2$/Al foil (cathode),

$LiPF_6$-based electrolyte, cleaned carbon cloth (shim) and a flexible aluminum (Al) soft packaging film. The final packaged full battery, consistent with the schematic of Figure 6(c) is exhibited in Figure 6(d–e), which reveals the excellent flexibility. The as-fabricated full battery was assembled and then cycled at 700 mA g^{-1} for 100 cycles. The mass loading of the active material of cathode and anode are approximately 13–15 and 1.5–1.8 mg cm^{-2}, respectively. The calculated capacities of cathode and anode (2*4 cm^2 pieces) are approximately 14.5–16.7 and 8.4–15.0 mAh, respectively. The cycle performance of the bent full batteries was shown in Figure 6(f). It can be observed that the initial discharge capacity is 1240 mAh g^{-1}, and decrease fast to 730 mAh g^{-1} after 10 cycles. The result indicated that the $LiCoO_2$ cathode does not fit well with the anode for the complete battery system. In the following cycles, the reversible discharge capacity remains stable with slight decrease. The bent full battery can still deliver a relatively high reversibility capacity of 500 mAh g^{-1} after 100 cycles even the performance of the anode was partly hindered by the $LiCoO_2$ cathode. To further demonstrate its practical application, we used the as-assembled full flexible battery to supply power under greatly bending state. Figure 6(g) shows that the bent flexible full battery can successfully lighten four lighting nixie tubes to display a pattern of "HUST", which is the initial of Huazhong University of Science and Technology.

It can be observed that external bending can hardly affect the performance of the flexible LIB with good stability and flexibility, which demonstrates its potential applications for future wearable/portable energy storage system.

In summary, we have prepared interconnected NiO nanosheets on highly flexible carbon cloth substrate as binder-free anode for LIBs through a simple solution method together with a post-annealing treatment. The obtained NiO nanosheets possess mesoporous feature which was confirmed by both TEM and BET. The integrated hierarchical 3D electrode shows many advantages such as large surface area, short diffusion length, good mechanical strength against volume change, fast ion and electron transport. The as-prepared electrode exhibited outstanding electrochemical performances such

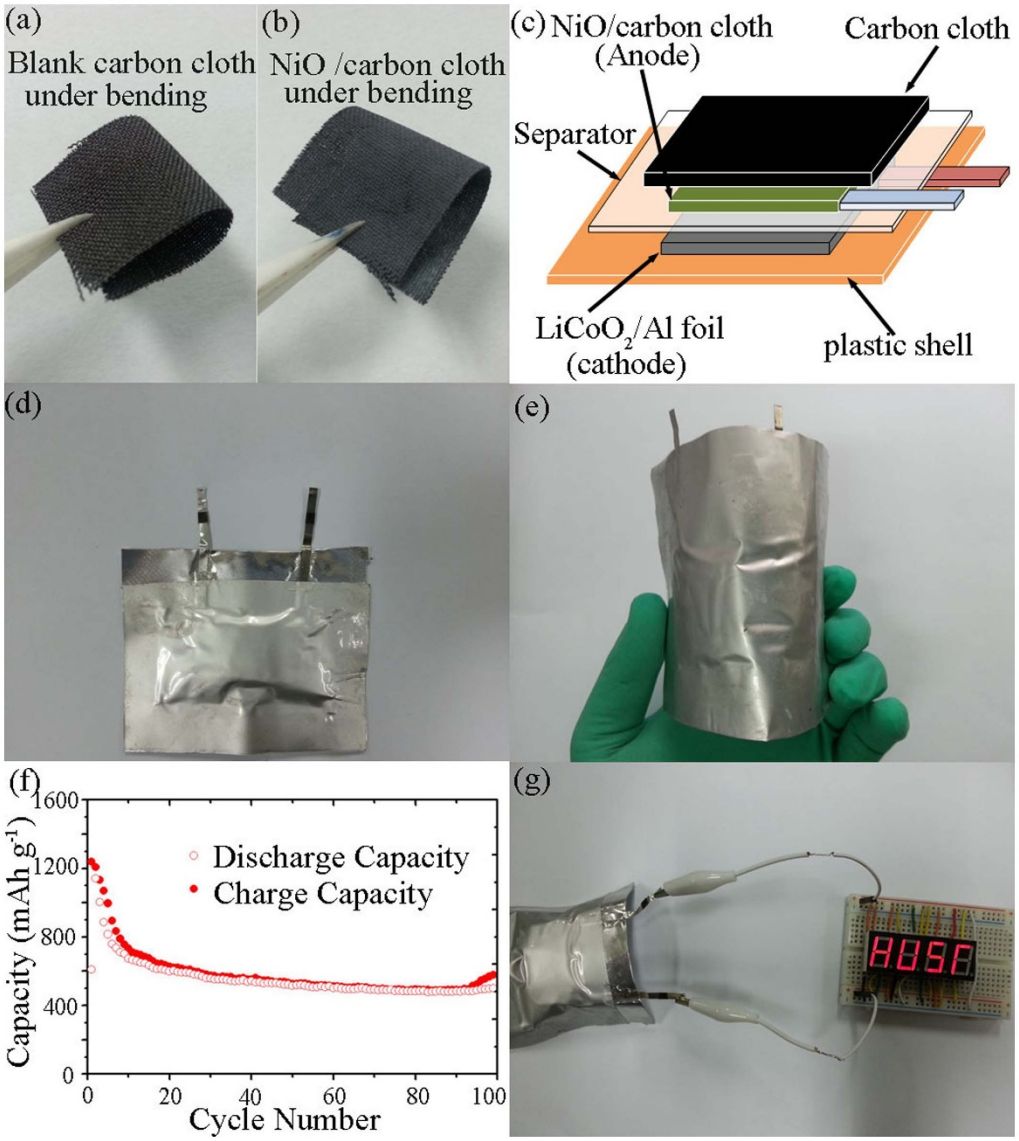

Figure 6 | Exhibition of the mesoporous NiO nanosheets/carbon cloth based flexible full LIBs. (a) Blank carbon cloth under bending. (b) Mesoporous NiO nanosheets/carbon cloth under bending. (c) Schematic of the mesoporous NiO nanosheets/carbon cloth based full LIB. (d–e) Photograph of full mesoporous NiO nanosheets/carbon cloth based LIB under non-bending and bending. (f) Cycling performance of the bent full LIBs based on NiO electrodes cycled at 700 mA g^{-1} in the voltage range of 1–4 V for 100 cycles. (g) Photograph of "HUST" pattern lightened by an as-assembled LIB under bending.

as high specific capacity (892.6 mAh g^{-1} after 120 cycles at 100 mA g^{-1}), excellent cycling stability (>98% Columbic efficiencies), long cycle-life (150 cycles) and good rate capability (758.1 mAh g^{-1} after 150 cycles at 700 mA g^{-1}). The electrode structure also possesses high flexibility, which was directly used as an anode to build flexible full battery. The battery demonstrated its flexibility by powering a commercial LED light and four nixie tubes respectively under bending state. The proposed fabrication approach and the 3D hierarchical integrated electrode design are promising for realization of high performance energy storage devices, especially for next-generation wearable/flexible electronic devices.

Methods

Synthesis of NiO nanosheets/carbon cloths. Carbon cloth with hydrophilic surfaces was purchased from Taiwan CeTech Co. Ltd. The $LiCoO_2$/Al foil used as cathode for full battery was purchased from Shenzhen Kejing Technology Co., LTD, and loading amount of $LiCoO_2$ powder is about 150 g m^{-2}. All chemicals are of analytical grade and commercially available, and are directly used without further purification.

A typical synthesis for mesoporous NiO nanosheets on carbon cloth was performed as following. The carbon cloth substrates were cleaned by sonication sequentially in acetone, ethanol and water for 30 min each. After being dried, the well-cleaned carbon cloth was placed vertically into Teflon-lined stainless autoclave of 100 ml capacity. 10 mmol $NiCl_2$ $6H_2O$, 40 mmol $CO(NH_2)_2$, 20 mmol NH_4F were dissolved in 100 ml of deionized water to form a homogeneous solution by constant stirring. After stirring for 1 h, the solution was transferred into the autoclave. The autoclave was sealed and maintained at 120°C for 7 h in an electric oven. After the autoclave cooled down to room temperature naturally, the sample was taken out, rinsed with ethanol and distilled water for several times, and dried in a vacuum oven at 60°C for 12 h. In the next step, the sample was put in a quartz tube and calcined at 350°C for 2 h with a ramping rate of 2°C min^{-1}.

Characterization. The morphology of the products was characterized by using field-emission scanning electron microscopy (FESEM, JEOL JSM-6700F) with an energy dispersive X-ray (EDX) attachment, transmission electron microscopy (TEM, FEI, Tecnai G^2 20) and field-emission transmission electron microscopy (FETEM, FEI, Tecnai G^2 F30). Crystal structure of products were characterized with X-ray diffractometer (XRD; X′ Pert PRO, PANalytical B.V., the Netherlands) with radiation from a Cu target (Kα, λ = 0.15406 nm). The ordering of mesostructure was analyzed by a lower-angle X-ray diffractometer system (RIGAKU D/MAX-RB, Japan) with a Cu Kα radiation source generated at 40 kV, 30 mA. Specific surface areas were computed from the results of N_2 physisorption at 77 K (Micromeritics ASAP 2020) by the Brunauer–Emmet–Teller (BET) and Barrett–Joyner–Halenda (BJH).

Electrochemical measurements. The electrochemical performance of the as-synthesized product was investigated by using it as a binder-free anode in LIBs in coin-type half-cells, which were laboratory-assembled by a CR2032 press in an argon-filled glove box with oxygen and water contents below 1 and 0.1 ppm respectively. A pure lithium foil was used as the counter electrode as well as reference electrode. A piece of NiO/carbon cloth was used directly as the working electrode, and Celgard 2400 polymer separator was employed. The electrolyte was 1 M $LiPF_6$ in ethylene carbonate (EC) and diethyl carbonate (DEC) (1 : 1 by volume). The cells were then aged for 12 h before the measurements to ensure full percolation of the electrolyte to the electrodes. Coin-type half-cells were cycled at various current densities and the voltage range of 0.01–3.0 V (vs Li^+/Li) at room temperature with a multichannel battery measurement system (Land, China). Cyclic voltammetry (CV) and electrochemical impedance spectra (EIS) experiment were conducted on an Autolab work station (PGSTAT-302N, Eco Echemie B.V. Company). The CV experiment was carried out in the range of 0.01–3.0 V (vs Li^+/Li) and at a scan rate of 0.1 mV s^{-1}. The EIS experiment was carried out at a frequency range of 0.01 Hz–100 kHz at an amplitude of 10 mV versus the open circuit potential.

The flexible full battery was assembled by using the NiO nansheets/carbon cloth as the anode, commercial $LiCoO_2$ as a cathode, 1 M $LiPF_6$ in a mixture of ethylene carbonate (EC) and diethyl carbonate (DMC) (1 : 1 by volume) served as the electrolyte, Celgard 2400 membrane as separator, and cleaned carbon cloth as shim to ensure contacting. The whole battery was packaged with Aluminum soft packaging film by heat-sealing. The full LIBs were assembled in an argon-filled glove box where oxygen and water concentration were strictly limited to below 1 ppm. The full cell was galvanostatically charged and discharged between 1.0 and 4.0 V versus Li^+/Li at room temperature with a multichannel battery measurement system (Land, China). The as-assembled full battery was charged to 4.0 V at room temperature with a multichannel battery measurement system (Land, China) before being used.

1. Tarascon, J. M. & Armand, M. Issues and challenges facing rechargeable lithium batteries. *Nature* **414**, 359–367 (2001).
2. Zhang, H., Yu, X. & Braun, P. V. Three-dimensional bicontinuous ultrafast-charge and-discharge bulk battery electrodes. *Nat. Nanotechnol.* **6**, 277–281 (2011).
3. Kang, K. S., Meng, Y. S., Breger, J., Grey, C. P. & Ceder, G. Three-dimensional bicontinuous ultrafast-charge and-discharge bulk battery electrodes. *Science* **311**, 977–980 (2006).
4. Arico, A. S., Bruce, P., Scrosati, B., Tarascon, J. M. & Schalkwijk, W. V. Nanostructured materials for advanced energy conversion and storage devices. *Nat. Mater.* **4**, 366–377 (2005).
5. Bruce, P. G., Scrosati, B. & Tarascon, J. M. Nanomaterials for rechargeable lithium batteries. *Angew. Chem. Int. Ed.* **47**, 2930–2946 (2008).
6. Lieber, C. M. & Wang, Z. L. Functional nanowires. *MRS Bull.* **32**, 99 (2007).
7. Kong, J. *et al.* Nanotube molecular wires as chemical sensors. *Science* **287**, 622–625 (2000).
8. Cui, Y., Wei, Q. Q., Park, H. K. & Lieber, C. M. Nanowire nanosensors for highly sensitive and selective detection of biological and chemical species. *Science* **293**, 1289 (2001).
9. Poizot, P., Laruelle, S., Grugeon, S., Dupont, L. & Tarascon, J. M. Nano-sized transition-metal oxides as negative-electrode materials for lithium-ion batteries. *Nature* **407**, 496–499 (2000).
10. Taberna, P. L., Mitra, S., Poizot, P., Simon, P. & Tarascon, J. M. High rate capabilities Fe3O4-based Cu nano-architectured electrodes for lithium-ion battery applications *Nat. Mater.* **5**, 567–573 (2006).
11. Bavykin, D. V., Friedrich, J. M. & Walsh, F. C. Protonated Titanates and TiO_2 Nanostructured Materials: Synthesis, Properties, and Applications. *Adv. Mater.* **18**, 2807–2824 (2006).
12. Lou, X. W., Deng, D., Lee, J. Y., Feng, J. & Archer, L. A. Self-supported formation of needlelike Co_3O_4 nanotubes and their application as lithium-ion battery Electrodes. *Adv. Mater.* **20**, 258–262 (2008).
13. Wu, B. H., Chen, J. S., Hng, H. H. & Lou, X. W. Nanostructured metal oxide-based materials as advanced anodes for lithium-ion batteries. *Nanoscale* **4**, 2526–2542 (2012).
14. Chen, J. S. & Lou, X. W. SnO_2 and TiO_2 nanosheets for high-performance lithium-ion batteries. *Mater. Today* **15**, 246–254 (2012).
15. Bavykin, D. V., Friedrich, J. M. & Walsh, F. C. Protonated titanates and TiO_2 nanostructured materials: synthesis, properties, and applications. *Adv. Mater.* **18**, 2807–2824 (2006).
16. Needham, S. A., Wang, G. X. & Liu, H. K. Synthesis of NiO nanotubes for use as negative electrodes in lithium ion batteries. *J. Power Sources* **159**, 254–257 (2006).
17. Wang, B., Cheng, J. L., Wu, Y. P., Wang, D. & He, D. N. Porous NiO fibers prepared by electrospinning as high performance anode materials for lithium ion batteries. *Electrochem. Commun.* **23**, 5–8 (2012).
18. Kim, G-P., Park, S., Nam, I., Park, J. & Yi, J. Electrospun NiO nanofibers as high performance anode material for Li-ion batteries. *J. Power Sources* **237**, 172–177 (2013).
19. Rai, A. K., Anh, L. T., Park, C. J. & Kim, J. Electrochemical study of NiO nanoparticles electrode for application in rechargeable lithium-ion batteries. *Ceram. Int.* **39**, 6611–6618 (2013).
20. Liu, L. *et al.* Nanosheet-based NiO microspheres: controlled solvothermal synthesis and lithium storage performances. *J. Phys. Chem. C* **114**, 251–255 (2010).
21. Bai, Z. C. *et al.* Direct large-scale synthesis of 3D hierarchical mesoporous NiO microspheres as high performance anode materials for lithium ion batteries. *Nanoscale* **6**, 3268–3273 (2014).
22. Wang, X. H. *et al.* NiO nanocone array electrode with high capacity and rate capability for Li-ion batteries. *J. Mater. Chem.* **21**, 9988–9990 (2011).
23. Caballero, A., Hernán, L. & Morales, J. A high-capacity anode for lithium batteries consisting of mesoporous NiO nanoplatelets. *Energy Fuels* **27**, 5545–5551 (2013).
24. Sasidharan, M., Gunawardhana, N, Senthil, C. & Yoshio, M. Micelle templated NiO hollow nanospheres as anode materials in lithium ion batteries. *J. Mater. Chem. A* **2**, 7337–7344 (2014).
25. Cheng, M.-Y. & Hwang, B. J. Mesoporous carbon-encapsulated NiO nanocomposite negative electrode materials for high-rate Li-ion battery. *J. Power Sources* **195**, 4977–4983 (2010).
26. Xia, Y. *et al.* Biotemplated fabrication of hierarchically porous NiO/C composite from lotus pollen grains for lithium-ion batteries. *J. Mater. Chem.* **22**, 9209–9215 (2012).
27. Zou, Y. Q. & Wang, Y. NiO nanosheets grown on graphene nanosheets as superior anode materials for Li-ion batteries. *Nanoscale* **3**, 2615–2620 (2011).
28. Huang, Y. *et al.* Self-assembly of ultrathin porous NiO nanosheets/graphene hierarchical structure for high-capacity and high-rate lithium storage. *J. Mater. Chem.* **22**, 2844–2847 (2012).
29. Zhou, G. M. *et al.* Oxygen bridges between NiO nanosheets and graphene for improvement of lithium storage. *ACS nano* **6**, 3214–3223 (2012).
30. Xie, D. *et al.* Synthesis of porous NiO-wrapped graphene nanosheets and their improved lithium storage properties. *J. Phys. Chem. C* **117**, 24121–24128 (2013).
31. Zhang, L., Wu, H. B. & Lou, X. W. Growth of SnO_2 nanosheet arrays on various conductive substrates as integrated electrodes for lithium-ion batteries, *Mater. Horiz.* **1**, 133–138 (2014).
32. Zhang, G. Q., Wu, H. B., Hoster, H. E., Chan-Park, M. B. & Lou, X. W. Single-crystalline $NiCo_2O_4$ nanoneedle arrays grown on conductive substrates as binder-free electrodes for high-performance supercapacitors. *Energy Environ. Sci.* **5**, 9453–9456 (2012).
33. Ripenbein, T., Golodnitsky, D., Nathan, M. & Peled, E. Electroless nickel current collector for 3D-microbatteries. *J. Appl. Electrochem.* **40**, 435–444 (2010).

34. Long, H. *et al.* Synthesis of nanowire self-assembled hierarchical $ZnCo_2O_4$ shell/Ni current collector core as binder free anodes for high-performance Li-ion batteries. *J. Mater. Chem. A* **2**, 3741–3748 (2014).
35. Wu, H. *et al.* Aligned NiO nanoflake arrays grown on copper as high capacity lithium-ion battery anodes. *J. Mater. Chem.* **22**, 19821–19825 (2012).
36. Liu, B. *et al.* Hierarchical three-dimensional $ZnCo_2O_4$ nanowire arrays/carbon cloth anodes for a novel class of high-performance flexible lithium-ion batteries. *Nano. Lett.* **12**, 3005–3011 (2012).
37. Liu, B. *et al.* Advanced rechargeable lithium-ion batteries based on bendable $ZnCo_2O_4$-urchins-on-carbon-fibers electrodes. *Nano Res.* **6**, 525–534 (2013).
38. Liu, B. *et al.* Hierarchical silicon nanowires-carbon textiles matrix as a binder-free anode for high-performance advanced lithium-ion batteries. *Sci. Rep.* **3**, 1622; DOI: 10.1038/srep01622 (2013).
39. Linares, N. *et al.* Mesoporous materials for clean energy technologies. *Chem. Soc. Rev.* Advance Article, DOI: 10.1039/C3CS60435G (2014).
40. Grugeon, S., Laruelle, S., Dupont, L. & Tarascon, J. M. An update on the reactivity of nanoparticles Co-based compounds towards Li. *Solid State Sci.* **5**, 895–904 (2003).
41. Poizot, P., Grugeon, S., Laruelle, S. & Tarascon, J. M. Rationalization of the low-potential reactivity of 3d-metal-based inorganic compounds toward Li. *J. Electrochem. Soc.* **149**, A1212–A1217 (2002).
42. Yu, Y., Chen, C. H., Shui, J. L. & Xe, S. Nickel-foam-supported Reticular CoO–Li_2O composite anode materials for lithium ion batteries. *Angew. Chem., Int. Ed.* **44**, 7085–7089 (2005).
43. Hu, Y. Y. *et al.* Origin of additional capacities in metal oxide lithium-ion battery electrodes. *Nat. Mater.* **12**, 1130–1136 (2013).
44. Hassoun, J., Lee, K. S., Sun, Y. K. & Scrosati, B. An advanced lithium ion battery based on high performance electrode materials. *J. Am. Chem. Soc.* **133**, 3139–3143 (2011).
45. Harris, S. J., Deshpande, R. D., Qi, Y, Dutta, I. & Cheng, Y.-T. Mesopores inside electrode particles can change the Li-ion transport mechanism and diffusion-induced stress. *J. Mater. Res.* **25**, 8 (2010).

Acknowledgments

This work is financially supported by National Science Foundation of China (No. 51275195 and 91323106) and by Program for Changjiang Scholars and Innovative Research Team in University (Grant no. IRT13017).

Author contributions

H.L., T.L.S. and Z.R.T. conceived the idea and co-wrote the paper. H.L. carried out the examples synthesis, characterization and electrochemical experiments. H.H. supported the synthesis, characterization and electrochemical experiments. S.L.J. and S.X. supported parts of characterization. All the authors discussed the results, read and approved the final manuscript.

Additional information

Supplementary information accompanies this paper at http://www.nature.com/scientificreports

Competing financial interests: The authors declare no competing financial interests.

How to cite this article: Long, H. *et al.* Growth of Hierarchal Mesoporous NiO Nanosheets on Carbon Cloth as Binder-free Anodes for High-performance Flexible Lithium-ion Batteries. *Sci. Rep.* **4**, 7413; DOI:10.1038/srep07413 (2014).